Impact of trace contaminants on SOFC operated with bio-syngas: sulphur and siloxane-induced degradation

Journal of Power Sources 665 (2026) 238967

Contents lists available at ScienceDirect

Journal of Power Sources

journal homepage: www.elsevier.com/locate/jpowsour

Impact of trace contaminants on SOFC operated with bio-syngas: sulphur and siloxane-induced degradation

Lucia Pera [a,*], Marta Gandiglio [a], Paolo Marocco [a], Davide Pumiglia [b], Livia Della Seta [b], Massimo Santarelli [a]

[a] Department of Energy, Politecnico di Torino, Corso Duca Degli Abruzzi 24, 10129, Torino, Italy
[b] ENEA - Italian National Agency for New Technologies, Energy and Sustainable Economic Development, Department of Energy Technologies and Renewable Sources (TERIN), Laboratory for Hydrogen and New Energy Vectors (H2V), Casaccia Research Centre C, Via Anguillarese 301, 00123, Roma, Italy

HIGHLIGHTS

- Long-term tests on button SOFC with bio-syngas containing trace contaminants.
- Effect of DMS, COS and D5 on SOFC under realistic fuel conditions.
- Sulphur species cause fast degradation by increasing charge transfer resistance.
- D5 induces slower degradation, mainly affecting mass transport processes.
- EIS, ECM, and DRT distinguish time-dependent electrochemical degradation.

GRAPHICAL ABSTRACT

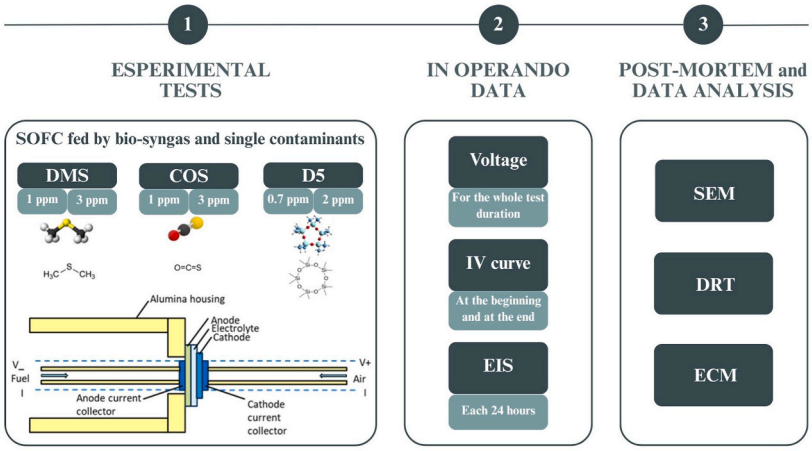

ARTICLE INFO

Keywords:
SOFC
Degradation
Bio-syngas
Dimethyl sulphide
Carbonyl sulphide
Decamethylcyclopentasiloxane

ABSTRACT

The energy valorisation of bio-syngas in Solid Oxide Fuel Cells (SOFCs) offers a highly efficient and sustainable alternative to conventional combustion-based systems. However, trace contaminants in syngas pose a challenge to long-term SOFC performance and durability (higher than in conventional ICEs). While most of previous works focused on hydrogen sulphide, other sulphur- and silicon-containing impurities, commonly found in bio-syngas, remain largely unexplored. This study investigates the impact of dimethyl sulphide (DMS), carbonyl sulphide (COS), and decamethylcyclopentasiloxane (D5), on the electrochemical performance of an anode-supported button-type SOFC operated with simulated bio-syngas at 750 °C. The degradation behaviour was assessed through periodic Electrochemical Impedance Spectroscopy (EIS), at different contaminant levels. Data were analysed using both equivalent circuit models and the Distribution of Relaxation Times (DRT) to distinguish degradation processes. Results reveal that sulphur-containing compounds significantly accelerate deterioration, primarily through increased charge transfer resistance associated with active site poisoning. In contrast, D5

* Corresponding author.
E-mail address: lucia.pera@polito.it (L. Pera).

https://doi.org/10.1016/j.jpowsour.2025.238967
Received 29 September 2025; Received in revised form 11 November 2025; Accepted 25 November 2025
Available online 9 December 2025

causes a more moderate degradation trend, attributed to increased mass transport limitations at low frequencies. This comprehensive study provides valuable insights into the degradation mechanisms induced by representative syngas contaminants and highlights the critical need for effective syngas purification strategies to enable the reliable deployment of SOFC systems in biomass-integrated energy applications.

1. Introduction

A Solid Oxide Fuel Cell (SOFC) is an electrochemical device that directly converts the chemical energy of a fuel into electricity through a high-efficiency, high-temperature process [1]. SOFCs are widely regarded as a highly efficient and versatile energy conversion technology, capable of operating with a variety of fuel sources, including hydrogen, natural gas, syngas and biomass-derived biogas [2]. The term bio-syngas refers to gas mixtures which can be obtained either from reforming of biogas (e.g. from anaerobic digestion) or from biomass gasification. In this context, gaseous biofuels are particularly attractive for power generation as controllable renewable energy sources when sourced from low-environmental impact feedstocks such as organic wastes, agricultural residues and manure. Reformed syngas, in particular, represents a promising fuel option due to its high hydrogen content and potential for integration with renewable energy systems. However, one of the main challenges associated with bio-syngas utilization in SOFCs is the presence of contaminants (e.g. sulphur and silicon compounds), which can lead to performance degradation and long-term operational instability [3]. A previous study by the authors [4] presented a comprehensive review of the impact of such contaminants across various energy conversion systems, with specific attention to their effects on SOFCs and other end-use applications. That work provided a broad overview of contaminant sources, types, and mitigation strategies, setting the foundation for the experimental investigation presented in this paper.

Sulphur-containing compounds are among the most critical contaminants in syngas, as they can poison the anode and significantly reduce the electrochemical activity of the cell, reacting with metal-based catalysts to form sulphides [4,5]. Several studies [6–8] have contributed to a deeper understanding of degradation mechanisms in SOFC anode, particularly in the presence of hydrogen sulphide (H_2S) and syngas as fuel. Additionally, several comprehensive reviews have addressed H_2S poisoning in SOFCs, summarizing the underlying mechanisms, recovery behaviour, and mitigation strategies [9,10]. Therefore, the present work does not aim to reproduce that extensive body of research. As shown in Table 1, only a selection of the most representative studies on H_2S is reported, particularly those involving bio-syngas compositions and similar electrochemical techniques, such as Electrochemical Impedance Spectroscopy (EIS), Distribution of Relaxation Times (DRT), and equivalent-circuit fitting.

Hagen et al. [11] conducted an experimental work to systematically study the impact of part per million (ppm) level H_2S in methane-containing fuels on SOFC anode performance and microstructure. They found that poisoning of the methane reforming reaction and anode electrochemical activity starts at low ppm levels of H_2S and worsens with increasing concentration, affecting particularly cell voltage and anode reaction sites. Hauch et al. [12] focused on the long-term H_2S exposure, demonstrating that low levels of contaminant cause reversible performance losses when operating at low anode overpotentials. On the other hand, at high overpotentials, irreversible long-term active sites that progressively occupy active sites essential for electrochemical reactions. Specifically, their study quantified the impact of this process on performance losses, correlating sulphur coverage with nickel deactivation.

Some other works have been conducted, and many of them identify 2 ppm of H_2S exposure as the maximum tolerable limit for the cell [3,7,

Table 1
Studies about experimental tests on SOFC with contaminants.

Author	Year	Contaminant analysed	Techniques	Cell	Reference
Hagen et al.	2011	H_2S 2–24 ppm	Voltage tracking SEM	ASC	[11]
Sasaki et al.	2011	H_2S 5 ppm Cl_2 5–1000 ppm D5 10 ppm	Voltage tracking FESEM	ESC	[17]
Weber et al.	2013	H_2S 0.5–15 ppm	Voltage tracking EIS DRT	ASC	[18]
Hagen et al.	2013	H_2S 2–8 ppm	Voltage tracking EIS	ASC	[19]
Hauch et al.	2014	H_2S 2 ppm	Voltage tracking EIS DRT SEM	ASC	[12]
Madi et al.	2015	D4 0.6–5 ppm	Voltage tracking EIS EDX	ASC	[16]
Papurello et al.	2018	H_2S 0.84–6.4 ppm HCl_2 1–1000 ppm D4 0.11–1.92 ppm	Voltage tracking	ASC	[7]
Pongratz et al.	2021	H_2S 1–10 ppm	EIS SEM and EDX	ESC and ASC	[6]
Kim et al.	2021	H_2S 0.5–1 ppm	EIS Raman	ASC	[20]
Yu et al.	2025	H_2S 3–5 ppm DMS 3–5 ppm	EIS DRT ECM	ESC	[14]
This work	2025	DMS 1–3 ppm COS 1–3 ppm D5 0.7–2 ppm	Voltage tracking EIS DRT ECM SEM and EDX	ASC	

13], with exposure beyond this point leading to irreversible degradation. Yu et al. [14] are among the first to consider the effect of dimethyl sulphide (DMS), alongside the more commonly studied H_2S, in their analysis of SOFC and recover. Nevertheless, studies focusing specifically on DMS remain scarce.

In addition, though the literature on H_2S is quite exhaustive, few studies focused on the degradation due to the presence of siloxanes. Among them, Papurello et al. [7] concluded that siloxanes reduce the anode porosity, and D4, taken as model siloxane, already acted at units of part per billion (ppb) levels on SOFC performance. Madi et al. [15,16] studied the degradation and recovery of anode-supported Ni-YSZ when fed with 5 ppm of D4, confirming that even trace contamination can affect the SOFC Ni-based anode. A summary list of the main experimental works about contaminant investigation on SOFC is shown in Table 1.

As shown in Table 1, to date, most studies on SOFC contamination have concentrated on the effects of hydrogen sulphide and D4, providing valuable insights into their adsorption behaviour and the resulted electrochemical degradation. In contrast, the effects of other sulphur- and silicon-containing compounds commonly found in bio-syngas, such as dimethyl sulphide (DMS), carbonyl sulphide (COS), and decamethylcyclopentasiloxane (D5), remains largely unexplored. Although typically present at lower concentrations than H_2S, these species may still significantly compromise SOFC durability due to their persistence and complex interactions with cell materials [15].

This study addresses this research gap by presenting a systematic investigation into the impact of DMS, COS, and D5 on SOFC degradation, providing mechanistic insights into how these contaminants influence processes, thereby supporting the development of mitigation strategies for real syngas applications. The novelty of the work lies not only in the selection of these specific underexplored compounds, but also in the comprehensive analytical approach adopted. The experimental campaign begins with a preliminary electrochemical characterization aimed at assessing the initial performance of a button cell (active area 2 cm^2) fed with simulated reformed syngas derived from biomass gasification. The fuel delivered to the anode is a pre-reformed, H_2/CO-rich stream model mixture ($H_2/CO/CO_2/H_2O/N2$). This composition was selected because the resulting molar fractions fall within the typical ranges reported in the literature for biomass-derived gas after reforming. The chosen mixture thus represents a generic, post-reforming syngas suitable for reproducible SOFC testing [21]. All tests are conducted on the same cell under realistic syngas conditions, operating at 750 °C under a constant current density of 0.5 A/cm^2. Each test is extended over a 120-h period. A comprehensive operando electrochemical characterization is carried out, by continuous voltage monitoring and measuring EIS spectra at discrete time intervals. The analysis of the spectra through DRT techniques to track the degradation dynamics under exposure to different contaminants and concentration levels is conducted. An equivalent circuit model is also applied to interpret impedance evolution and gain insight into the underlying electrochemical processes.

By clarifying the degradation mechanisms induced by these impurities, the findings provide critical insight into SOFC performance under practical conditions. This contribution supports the development of more robust fuel cell systems and highlights the importance of targeted purification strategies for real-world applications.

The paper is structured as follows. Section 2 details the methodology, explaining the experimental procedure and including electrochemical techniques employed for the tests. Section 3 presents and discusses the results obtained from exposure to each of the selected contaminants (DMS, COS and D5), including performance trends, impedance evolution, and the outcomes of equivalent circuit modelling. This section concludes with a post-mortem analysis of the cell carried out via Scanning Electron Microscopy (SEM), which supports the interpretation of the electrochemical results and provides insights into the underlying degradation mechanisms. Finally, Section 4 summarises the key conclusions of the study.

2. Methodology

2.1. Experimental procedure

The experimental campaign utilises a test station equipped with advanced components to ensure precise operation and monitoring. The system includes a temperature-controlled furnace, Mass Flow Controllers (MFCs) for managing gases, both at anode and cathode side. Anodic gas humidification is achieved using a Controlled Evaporator Mixer (CEM), which is coupled with a liquid flow controller. The system supplies the desired amount of superheated steam into the fuel stream. Water is supplied to the liquid flow controller from a reservoir pressurized with nitrogen gas, ensuring stable and continuous operation.

Power management is facilitated by a BK precision 9201 power supply, while the electronic load is a BK precision 8600 DC, alongside a data logger and control software based on LABVIEW. Electrochemical Impedance Spectroscopy (EIS) is conducted using EC-Lab® software for Windows, developed by BioLogic for Potentiostat/Galvanostat instruments.

SOFC button cell sample is mounted on a cylindrical alumina support and fixed on top of it using a high-temperature refractory paste. After being thermally treated according to the manufacturer's specifications, the paste ensures that the cell remains immobilised and effectively seals the air and fuel chambers, preventing gas leaks. The cell is held vertically, and two current collectors – one consisting of a nickel mesh for the anode side, and the other of a gold mesh for the cathode side – are placed in contact with the respective electrodes of the sample in an open-electrode configuration. A thermocouple for monitoring the cell temperature is positioned in the proximity to the sample. Each gas stream (N_2, H_2, CO_2, CO) is regulated using a dedicated mass flow meter. Separate supply lines are employed for introducing trace contaminants, allowing precise dosing. All gases and contaminants are premixed before entering the system through the anode inlet. Fig. 1a provides a schematic representation of the test bench layout, while a summary of the methodology developed in this work is graphically summarised in Fig. 1b.

Electrochemical performance tests are conducted on commercial anode supported button cells with a 2 cm^2 active area (details in Table 2).

Before starting the test with contaminated bio-syngas, the reduction of NiO to Ni in the anode is achieved by supplying a 5/95 %vol H_2/N_2 gas mixture to the anode, gradually increasing the content of H_2 up to 100 %vol H_2. The total gas flow rate is maintained at 150 ml/min. Prior to applying a constant current to the cell, its basic electrochemical performance and the impedance spectra are evaluated using a 50/50 % vol H_2/N_2 mixture.

Fuel cell is tested under ambient pressure and at constant operating temperature of 750 °C, with air supplied to the cathode. On the anode side, a model reformate gas mixture is provided to the cell [22], including H_2, CO, CO_2, H_2O, N_2 with the composition listed in Table 3. The total anode flow rate is 150 ml/min, whereas the air electrode receives a steady flow of 300 ml/min of air, ensuring an oxygen surplus. The fuel electrode flow rate is intentionally maintained at a level significantly higher than the stoichiometric requirement associated with the applied current. This strategy ensures optimal operating conditions by preventing local fuel starvation and preserving stable cell performance throughout the test. To establish a reference baseline, a preliminary test is carried out using clean bio-syngas, so that any additional degradation observed in subsequent tests can be more confidently attributed to the presence of contaminants.

For contamination tests, the base bio-syngas is pre-mixed with a single contaminant species before entering the anode side. As shown in Fig. 1b, each contaminant is tested individually at two representative concentration levels, low and high. Specifically, DMS and COS are selected as representative sulphur-containing compounds, while D5 is used as a model siloxane. The corresponding concentrations are detailed

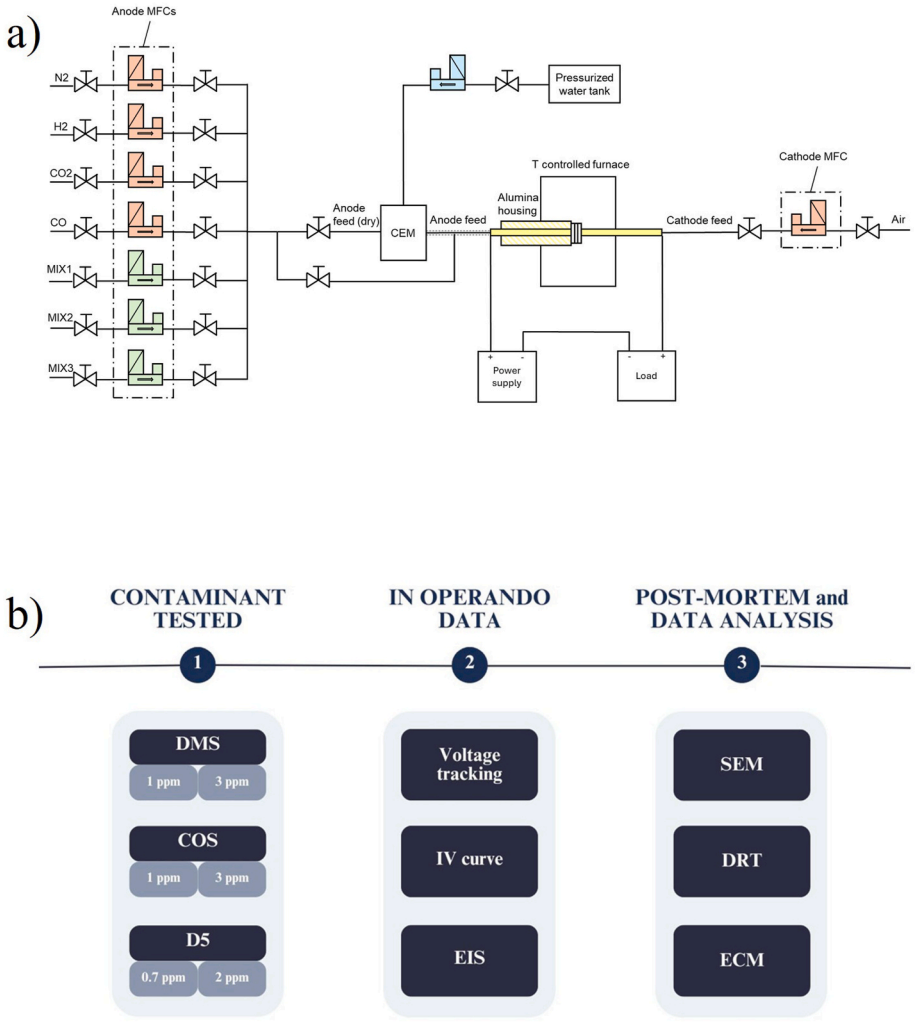

Fig. 1. a) Diagram of the test station, b) Methodology of the work.

Table 2
Material and thickness of each cell layer.

Parameter	Layer material	Value
Fuel electrode thickness	Ni/8YSZ	500 ± 20 μm
Electrolyte thickness	8YSZ	30 ± 10 μm
Barrier layer	GDC	4 ± 2 μm
Air electrode thickness	LSCF/LSC	8 ± 2 μm

Table 3
Reference syngas operating conditions.

Anode					
Components	H_2	CO	CO_2	H_2O	N_2
Composition (%vol)	45 %	24 %	11 %	18 %	2 %
Cathode					
Components	O_2			N_2	
Composition (%vol)	21 %			79 %	

in Table 4.

The experimental campaign focuses on real-time electrochemical monitoring over an evaluation lasting 120 h, aimed at assessing mechanism changes during long-term operation with contaminated biosyngas under polarised conditions. The test maintains constant parameters such as temperature, fuel electrode flow rate, and gas composition.

Table 4
Summary of tested contaminant levels.

DMS		COS		D5	
Low	High	Low	High	Low	High
1 ppm	3 ppm	1 ppm	3 ppm	0.7 ppm	2 ppm

As illustrated in Fig. 1b, a combination of voltage tracking, IV characterization and EIS is employed to monitor the cell's performance and degradation behaviour in detail. Throughout the experiment, the cell voltage is continuously tracked, while electrochemical impedance spectroscopy is performed every 24 h in order to appreciate the variation in time. Polarised EIS measurements are essential as they simulate the real operational environment of bio-syngas-fuelled solid oxide fuel cells in stationary use, avoiding harsher contamination effects due to Open Circuit Voltage (OCV) operation. In fact, the formation of water vapor limits irreversible contamination which may occur on the active surface of the fuel electrode [23], especially for species prone to hydrolysis reactions. Moreover, anodic polarization acts as a limiting factor for sulphur-related poisoning processes. These operando measurements are performed under polarization of 1 A and use a four-probe connection involving a variation of 200 mA AC signal across frequencies ranging from 100 kHz to 10 mHz, with 10 data points collected per decade of frequency.

Polarization curves are carried out at the beginning and at the end of

the test by increasing the current density stepwise, from OCV until the cell's voltage drops below 700 mV in order to avoid the re-oxidation of the nickel. Each experiment is repeated until consistent electrochemical responses are obtained, and the data reported herein are representative of the most reproducible results. The testing sequence begins with clean syngas to establish a baseline, followed by exposure to DMS (1 and 3 ppm), COS (1 and 3 ppm), and finally D5, maintaining identical operating conditions throughout the entire campaign.

To further investigate degradation mechanisms, the electrochemical data are post-processed (Fig. 1b) through DRT and ECM, allowing the deconvolution and quantification of individual physicochemical contributions. Additionally, post-mortem analyses via SEM and EDX are conducted on the tested samples to assess possible structural changes or contaminant accumulation on the cell surface. These combined methodologies offer a comprehensive understanding of performance losses and their correlation with specific degradation phenomena.

2.2. Equivalent circuit model

As proposed by Boigue Muñoz et al. [24], experimental data from EIS spectra are fitted through an Equivalent Circuit Model (ECM) to simulate the cell operation from its electrochemical point of view. This circuit can be utilised for simultaneous Complex Non Linear Square (CNLS) fitting of experimental impedance data, enabling the determination of circuit element values and, consequently, the electrochemical parameters characterising the SOFCs examined in this study.

For experimental tests including contaminant in the feed, the corresponding equivalent circuit model commonly used is shown in Fig. 2.

R_0 represents the cell's ohmic resistance, encompassing the various electronic and ionic resistances connected in series. However, the dominant factor influencing R_0 is the conductivity of the electrolyte layer, as its resistance is significantly higher compared to that of the electrodes.

An RC parallel is commonly employed to describe the EIS response associated with charge transfer at the Three-Phase Boundary (TPB) interface. However, under non-ideal conditions, such as distributed surface reactivity, surface inhomogeneity, roughness, or fractal geometry, a constant phase element (CPE) is preferred over a traditional capacitor for fitting purposes. The CPE effectively captures deviations from ideal capacitive behaviour in the EIS response by incorporating an exponential factor, n, where $0 \leq n \leq 1$ [25]. Two anodic processes (charge transfer reaction and ionic transport) and a cathodic process are represented with a parallel RCPE [26,27]. The parameters $R_{ct,an,1}$ and $R_{ct,an,2}$ correspond to the charge transfer and ionic transport resistances at the anode, while $R_{ct,cat}$ is the charge transfer resistance at and cathode TPB. $CPE_{ct,an}$ and $CPE_{ct,cat}$ represent the double-layer capacitances at the interfaces between the electronic and ionic conducting phases in both the anode and cathode.

The diffusion of gaseous species within a solid porous structure is typically modelled using a finite-length Warburg (FLW) diffusion impedance [28]. In ECM, W_{an} and W_{cat} represent the gas diffusion through anode and cathode porous matrix, respectively. In most cases, particularly when normal or oxygen-enriched air is supplied to the cathode, the impact of diffusion process at cathode is minimal or obscured by other overlapping contributions [29]. As a result, its impedance W_{cat} has been disregarded in our work.

Regarding the process which corresponds to the water-gas shift reaction occurring exclusively when syngas is used as fuel, previous studies indicate that its behaviour is primarily governed by gas conversion rather than by gas diffusion [22]. Consequently, for fitting purposes, a parallel R-CPE circuit provides a more accurate representation than a distributed element.

Lastly, an inductive element L_0 is included to account for the high-frequency inductive impedance caused by instrumental electrical artifacts.

Each circuit element value is determined through the ZView software [30] through complex nonlinear least squares fitting. In particular, the extracted values of the resistances correspond to distinct physicochemical processes identified in the DRT analysis. By tracking these resistances over time, it is possible to identify which processes are most affected during cell operation.

3. Results and discussion

As a preliminary step, a Long Term clean Syngas (LTS) test was performed to establish a reference benchmark for all subsequent tests involving contaminants. The main outcomes of this baseline experiment are reported in the Supplementary Material, as the primary objective of the study is to evaluate the effects induced by specific impurities. Nonetheless, it is worth highlighting that, in the absence of contaminants, the cell exhibited a rather stable voltage profile, with only a minor drop of approximately 5 mV observed in the final phase of the test, after 90 h of operation. This slight degradation can be justified by considering that our test duration was limited to 120 h, whereas other long-term experimental studies [31,32] have reported fluctuations in both positive and negative directions, with a more pronounced initial decay occurring within the first hours of operation, typically followed by stabilisation. Alternatively, the slight voltage loss may also be associated with carbon deposition phenomena, potentially linked to the Boudouard reaction [33,34]. The resistances of each process are constant in time, and no variation is pointed out from EIS plot during the test duration.

3.1. Operando results

Fig. 3a illustrates the temporal evolution of the voltage variation (ΔVoltage) expressed in millivolts (mV) as a function of time, measured in hours (h), under two different concentrations of DMS: 3 ppm and 1 ppm. The blue curve corresponds to the measurements obtained at a concentration of 3 ppm, while the red curve represents the data collected at 1 ppm. The voltage variation is plotted relatively to the initial voltage value, registered as the contaminant is injected, enabling a direct comparison of the electrochemical behaviour under the two test conditions. Both data series exhibit a general downward trend over time, which may be associated with the degradation of the electrochemical system, or the evolution of specific reactions influenced by the presence of DMS. At the onset of the experiment, the voltage drop is particularly steep for the 3 ppm case, suggesting a more rapid response to the presence of DMS at higher concentrations. This initial sharp decline (from 0 to 5 h of operation) is followed by a slower, more gradual decay phase, as observed also by Yu et al. [14]. In contrast, the 1 ppm curve exhibits a less pronounced and more stable decline, indicative of a more controlled electrochemical behaviour. Overall, the trend suggests that increasing the concentration of DMS accelerates the voltage decay process. After 120 h of operation, the voltage degradation with 1 ppm is 20 % lower than the 3 ppm case. These observations could imply a concentration-dependent mechanism influencing the electrochemical

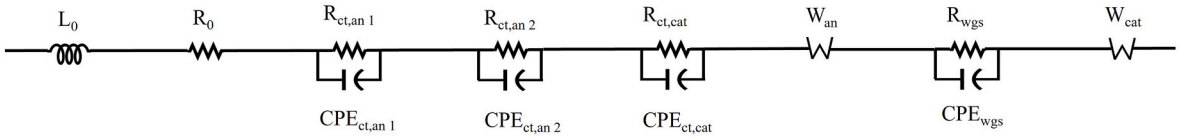

Fig. 2. Equivalent circuit model.

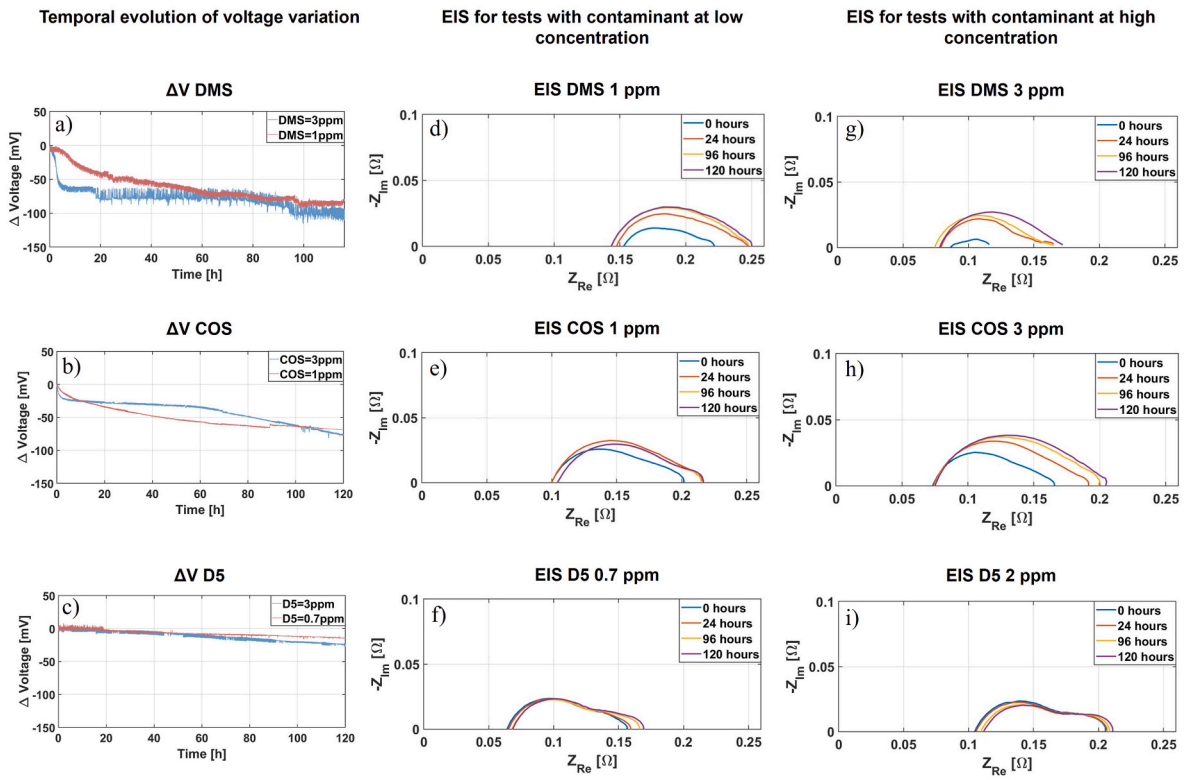

Fig. 3. Temporal evolution of voltage variation: a) Tests with DMS = 3 ppm and DMS = 1 ppm, b) Tests with COS = 3 ppm and COS = 1 ppm, c) Tests with D5 = 2 ppm and D5 = 0.7 ppm. EIS recorded for test with: d) low level concentration of DMS, e) low level concentration of COS, f) low level concentration of DMS, g) high level concentration of DMS, h) high level concentration of COS, i) high level concentration of D5.

characteristics, such as adsorption kinetics, reaction pathways, or degradation processes.

More information on the DMS-related degradation mechanisms for the two samples arise from the analysis of the EIS spectra (Fig. 3d and g). For the sake of clarity in graph interpretation, although the EIS measurements were taken every 24 h, only four have been selected to clearly illustrate the trend. At the initial time (0 h), the Nyquist plot for the 1 ppm test exhibits an arc at high frequency and a smaller one at low frequency. As the exposure time increases, the ohmic resistance is reduced by the improvement of the material conductivity [7] and there is a progressive enlargement of the high frequency arc. Notably, significant changes appear after 24 h of exposure, with the impedance spectrum at 24 h showing marked differences compared to the initial state. In contrast, the spectra at 96 ad 120 h exhibit similar trends to that at 24 h, suggesting that the degradation process tends to stabilize or reach a saturation state beyond this point at the tested DMS concentration. This trend indicates a temporal increase in the charge transfer resistance. The maximum of the semicircle also shifts slightly toward higher values on the real axis over time, reinforcing the interpretation of increased resistance. The imaginary part of the impedance likewise increases, suggesting more pronounced capacitive behaviour as degradation progresses.

The comparison with the corresponding EIS results obtained under 3 ppm DMS exposure reveals a similar qualitative evolution, showing a leftward shift of the spectra along the real axis likely due to conductivity improvement. This decrease in ohmic resistance may be explained by a progressive enhancement of the electrical contact between the current collector and the outer Ni layer on the anode surface. When the cell is operated at a given current density for a certain time, the local temperature rise induced by the Joule effect promotes stronger adhesion between the current collector and the Ni phase, especially in a horizontal setup such as ours, where the initial contact is not favoured by gravity. Such an effect is particularly evident after the first 24 h, suggesting that the cell might not have been allowed sufficient time to fully stabilize before the start of the measurement campaign.

In parallel, the spectra also show an increase in the arc radius at high frequency as a function of operation time. In particular, the effects are more pronounced in 3 ppm case, particularly between 0 and 24 h, where the semicircle enlargement is noticeably greater. This indicates a more significant degradation at higher DMS concentration, likely driven by a more rapid and aggressive interaction with the catalyst layer. Despite this, both concentrations appear to exhibit a form of degradation plateau beyond 96 h, as evidenced by the minimal changes between the 96-h and 120-h spectra. The similarities in the later-stage behaviour at both DMS concentrations may suggest that the system approaches a limiting state of degradation, beyond which further performance loss becomes marginal.

Overall, the evolution of EIS response over time provides clearly evidence of degradation. The immediate increase in high frequency arc, is caused by the release of sulphur-containing fragments which then strongly adsorb onto the nickel catalyst, blocking the active sites [14]. This effect appears within the first few hours of operation and progressively diminishes with longer exposure. As observed for low level DMS, also for the high level test the slight decrease in ohmic resistance observed during the DMS exposure is attributed to improved electrical contact between cell and collectors, rather than to the contaminant itself. This effect likely reflects a stabilisation of the cell assembly, which can vary slightly among samples due to the vertical configuration of the setup.

Similar to the behaviour observed with DMS, COS exposure also leads to a voltage drop during the initial hours of operation (Fig. 3b). In the 3 ppm test, the initial decline is more pronounced (24 mV within the first 5 h of operation), followed by a period of relative stability. However, after approximately 70 h, the voltage begins to gradually decrease again. In contrast, the 1 ppm test exhibits a more subtle (17 mV within the first hours of operation) and continuous decline over the entire test

duration.

The EIS spectra (Fig. 3e and h) closely reflect these trends, showing an initial rapid increase in charge transfer resistance within the first 24 h, followed by a slower but steady rise in total polarization resistance. In both cases, the ohmic resistance remains essentially unchanged, as indicated by the stable high-frequency intercept across all spectra. This suggests that the electrolyte, current collectors, and interfacial contacts maintain consistent conductivity throughout the 120-h test.

The lower total resistance observed at 3 ppm compared to 1 ppm is attributed to slight differences in cell assembly and contact quality, which affect the initial ohmic resistance. Minor misalignment of the collectors or imperfect sealing of the ceramic adhesive may cause small H_2 leakages and alter the initial EIS shape. These effects are purely mechanical and do not reflect the influence of the contaminant concentration. Nevertheless, both COS and DMS tests at higher concentration show a larger increase in polarization resistance over time, confirming the stronger impact of contaminant exposure.

Given that COS belongs to the same chemical class as DMS and produces comparable electrochemical responses, it is reasonable to infer that sulphur-induced degradation likely follows a similar mechanism, primarily involving the blockage of active sites at the anode. However, COS exposure induced a dynamic response, with multiple changes in the slope of the voltage curve. This can be attributed to the dual behaviour of COS: it can both adsorb directly on Ni forming Ni–S bonds and undergo hydrolysis [35] in the presence of steam to form $H_2S + CO_2$. The latter reaction is catalysed by Ni surfaces and is promoted at high temperature and steam content. While this pathway generates H_2S, which is a stronger poison for Ni catalysts, it is also known that steam can contribute to the partial removal of adsorbed sulphur [36]. By promoting the desorption of H_2S and preventing its deposition as sulphate or elemental sulphur, H_2O helps maintain catalyst activity and stability [37]. The resulting interplay between formation of H_2S and potential sulphur desorption introduces a dynamic equilibrium that manifests in the transient performance. In contrast, DMS (CH_3–S–CH_3) lacks the polarised C=O bond present in COS and is therefore less prone to hydrolysis. Its behaviour can be mainly described as surface-mediated dissociative adsorption on Ni, releasing sulphur atoms that form Ni–S bonds and methane as a by-product, as also reported under H_2-rich reducing conditions [14]:

$$(CH_3)_2S + H_2 \rightarrow H_2S + 2CH_4 \quad (1)$$

This mechanism leads to a rapid saturation of Ni active sites by sulphur and thus to a quasi-steady degree of deactivation, more similar to that induced by H_2S at comparable concentrations.

Although thermal decomposition of both COS and DMS is thermodynamically possible, it is not expected to play a major role under the present conditions. The contaminants are introduced at ppm levels into a reactive gas mixture (H_2, H_2O, CO, CO_2, N_2) with very short residence time before reaching the anode, which makes homogeneous gas-phase decomposition kinetically limited. Instead, the observed behaviour can be attributed primarily to surface-mediated reactions (adsorption, hydrolysis, and dissociation) occurring at the Ni anode.

The D5 voltage graph in Fig. 3c shows the progressive decline in cell voltage over time for both curves. With respect to the DMS and COS voltage trends, the voltage drops relatively moderate and linear [7], with only minor fluctuations throughout the duration of the test. A difference in the voltage decay profiles between the two concentrations is observed, revealing the concentration-dependent impact on SOFC performance.

In the case of 0.7 ppm D5, the curve exhibits a relatively gradual decline over time, indicative of a mild degradation process. Conversely, the cell exposed to the higher concentration (2 ppm) shows a more pronounced voltage decline, especially in the last hours of operation. While the degradation of SOFCs exposed to siloxane-contaminated fuels is clearly time-dependent [38,39], exhibiting progressive performance losses with increased operation duration, it is also influenced by the contaminant concentration. Higher D5 levels result in more severe degradation [15], although beyond a certain threshold the marginal effect of increasing concentration diminishes, pointing toward a complex interplay between time-dependent surface poisoning and concentration-driven adsorption kinetics.

The EIS data for the 0.7 ppm D5 test (Fig. 3f) reveal subtle but progressive modifications in the impedance response over time, reflecting the evolving impact of siloxane exposure on the cell's electrochemical performance. At the initial stage (0 h), the impedance arc presents the lowest magnitude, indicating minimal polarization resistance. As the operating time increases, a gradual enlargement of the intermediate-to-low frequency arc is observed. The shapes of the arcs remain relatively consistent, implying that the overall cell structure and transport pathways are not drastically altered within the first 120 h.

Comparable trends to those observed at lower concentrations can be identified also for the 2 ppm test (Fig. 3i); however, a notable difference lies in the behaviour of the high-frequency intercept with the real axis. Specifically, a rightward shift is observed after 24 h of operation, followed by a gradual increase over the subsequent hours, reaching a higher value by 120 h.

As reported by Haga et al. [40], the precipitation of silica can significantly reduce the active TPB areas. This reduction leads to a simultaneous increase in both non-ohmic anodic polarization and ohmic resistance on the anode side. In addition, results from SOFCOM project have shown that silica may also deposit on metallic surfaces such as interconnects or current collectors, thereby increasing the ohmic resistance [3]. Evidence of this behaviour can be observed in the EIS data from test conducted with 0.7 ppm of D5, where the gradual increase in the x-axis intercept indicates a rise in ohmic losses over time. The formation of $SiO_2(s)$ occurs through the following reactions:

$$[(CH_3)_2SiO]_5(g) + 25H_2O \rightarrow 5Si(OH)_4(g) + 10CO + 30H_2 \quad (2)$$

$$Si(OH)_4(g) \rightarrow SiO_2(s) + 2H_2O \quad (3)$$

According to Madi et al. [15], siloxanes rapidly decompose upon entering the anode chamber of the fuel cell, leading to the deposition of silica on the anode surface and extending to the electrolyte interface. Their work focused on evaluating the durability of Ni-YSZ anode-supported cells exposed to D4 impurity using a simulated-reformate fuel. The study showed irreversible degradation associated with silica formation, supported by thermodynamic calculations that identified two possible pathways for partial volatilization of the deposited SiO_2(s) as SiO(g).

Although the two compounds (D4 and D5) differ slightly in molecular weight and volatility, they share similar chemical structures and decomposition mechanisms, leading to the formation of Si-containing intermediates such as $Si(OH)_4$ and SiO_2 under high-temperature and steam-rich conditions. Therefore, the mechanisms proposed by Madi et al. can be reasonably extended to D5. In the presence of reformed biogas, deposited $SiO_2(s)$ can undergo a reduction reaction, forming

Table 5
Voltage variation (ΔVoltage) for test with contaminant at low and high concentrations.

	Initial degradation (5 h)	Long-term degradation (5–120 h)	Total degradation (0–120 h)
DMS			
low	11 mV	69 mV	80 mV
high	60 mV	40 mV	100 mV
COS			
low	17 mV	49 mV	66 mV
high	24 mV	55 mV	79 mV
D5			
low	1 mV	14 mV	15 mV
high	2 mV	22 mV	24 mV

volatile *SiO* gas [16], as shown below:

$$2SiO_2(s) + H_2(g) + CO(g) \rightarrow 2SiO(g) + H_2O(g) + CO_2(g) \quad (4)$$

Although this reaction has not been directly evidenced in our experiments, it represents a plausible pathway for partial silica volatilization under the reducing conditions of SOFC operation. This volatile SiO could be transported further into the fuel stream and the porous anode structure. Despite this possible volatility, silica accumulation is still expected to occur locally, reducing the active TPB area and hindering gas diffusion, as reflected in the EIS by the enlargement of the second arc, indicating increased mass-transport limitations.

Table 5 summarises the voltage degradation observed for each contaminant at both concentration levels. Notably, sulphur-containing compounds at high concentrations exhibit a pronounced drop during the initial hours of operation. In contrast, D5 leads to a more gradual and less severe decline over time. Initial and final OCV values of each test can be found in the Suppementary Material.

3.2. Resistances evolution

The temporal evolution of each resistance is summarised in Table B.1. Since each test was performed on a different cell, the absolute values of the resistances should not be directly compared, as they can be influenced by several factors such as differences in cell assembly, electrode contact quality, sealing conditions and microstructural variability.

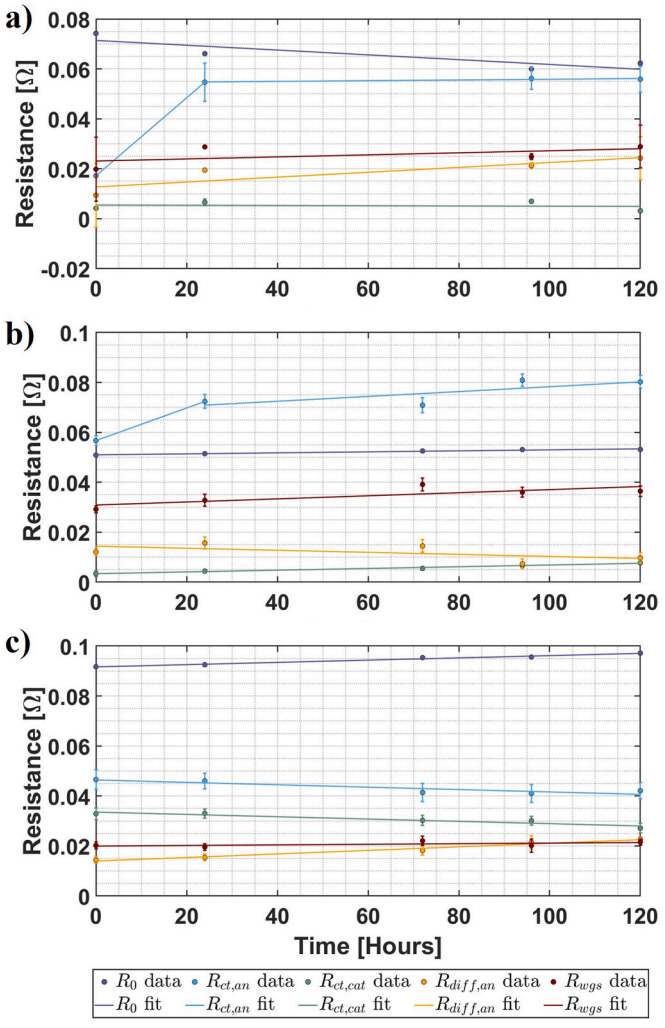

Fig. 4. Resistances evolution over time for test with: a) 3 ppm of DMS, b) 3 ppm of COS, c) 2 ppm of D5.

The resistance trends and error bars over time for tests with individual contaminants at high concentrations are shown in Fig. 4, while low concentrations trends are reported in Supplementary material. Notably, the dominant limitation to cell performance under DMS and COS exposure is consistently the anodic charge transfer resistance ($R_{ct,an}$), which shows the highest variation over time (light-blue line in Fig. 4a–b). Other contributions from the anode side, such as gas diffusion through the porous electrode (yellow line) and the water-gas shift reaction (red line), remain relatively stable. Similarly, the cathodic charge transfer resistance (green line) remains constant over time, while the ohmic resistance R_0 (blue line) slightly decreases, in agreement with trends observed in the impedance spectra. Notably, the fitting of the anodic charge transfer resistance is segmented into two parts. This choice is justified by the evolution observed in the impedance spectra, particularly within the first 24 h of operation. After 24 h, the arc's shape and size become more stable, as seen in the 96 and 120-h curves, which supports the observed stabilisation of $R_{ct,an}$ in the resistance fit over time. This rapid initial increase suggests an early degradation or poisoning mechanism affecting the anode side, likely due to sulphur species from DMS and COS.

This correlation between resistance fitting and EIS data reinforces the interpretation that the anodic charge transfer process is the most affected in the presence of sulphur compounds and highlights the importance of time-resolved analysis for understanding degradation phenomena in fuel cells.

On the other hand, siloxanes exposure reveals distinct resistance trends (Fig. 4c). $R_{ct,an}$ demonstrates a gentle, gradual decrease over the entire duration. This behaviour aligns with impedance spectra exhibiting stable, slowly evolving arcs without abrupt changes. The absence of immediate and significant growth in anodic charge transfer resistance further indicates that siloxane primarily impacts diffusion processes, reinforcing the importance of contaminant-specific impedance analysis in distinguishing degradation mechanisms. Notably, an increase in the anodic diffusion resistance is observed, as previously discussed in the EIS analysis. The trend is also consistent with previous research by Tian et al. [38], who reported significant silica formation from D4 decomposition, causing pore blockage and thereby progressively increasing diffusion limitations at the anode. Our results are also in line with the observations of Sasaki et al. [17], who fed 10 ppm D5 to Ni-cermet SOFCs and recorded a gradual voltage decay. They attributed this performance loss to SiO_2 precipitation concentrated near the gas-exposed surface of the porous anode, which progressively blocks gas pathways and mirrors the monotonic rise of $R_{diff,an}$ seen in the present study.

3.3. Distribution of relaxation times

The DRT spectra (Fig. 5) provide further insight into the electrochemical processes already discussed in the previous sections. Each profile reveals the presence of at least five distinct relaxation processes, characterized by different frequency domains. Depending on the fuel composition and operating temperature, partial overlapping of processes may occur, especially when their characteristic frequencies differ by less than one order of magnitude. Overlapping between adjacent processes is expected, however, according to prior studies [27–29,41,25] frequency regions can be generally attributed as follows:

- 1 Hz: gas conversion under reforming gas operation and/or oxygen electrode adsorption/desorption;
- 1–10 Hz: fuel electrode gas diffusion in pores;
- 10–1000 Hz: oxygen electrode charge transfer and oxygen ions diffusivity;
- 1000–10000 Hz: attribution to fuel electrode charge transfer reaction and ionic transport;
- $>$ 10 kHz: only seen for measurement conducted at high frequency, and no consensus exists in literature.

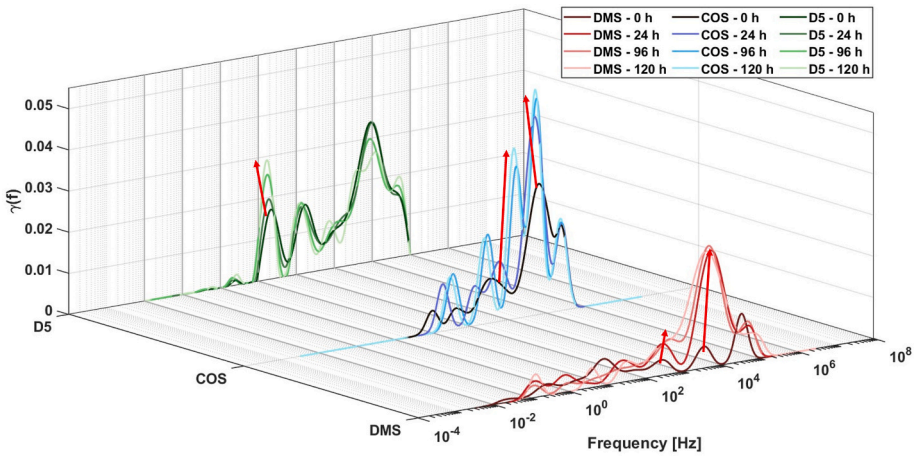

Fig. 5. DRT for tests with 3 ppm of DMS, 3 ppm of COS, 2 ppm of D5. Red arrows show the main variations. (For interpretation of the references to colour in this figure legend, the reader is referred to the Web version of this article.)

As shown in Fig. 5, for DMS (red curves), the most significant relaxation process occurs in the high frequency range (~1000–10000 Hz), and it exhibits a clear and progressive increase in intensity over time. This trend suggests a growing contribution of charge transfer resistance at the fuel electrode, likely due to active site poisoning. COS (blue lines) displays a similar behaviour though the increase is slightly more gradual, with the main peak shifting slightly toward lower frequencies.

Conversely, the DRT spectra for D5 (green curves) remain mostly unchanged throughout the 120-h exposure, with peak intensities showing minimal variation. The only notable change is a subtle fluctuation in the low-frequency range (~10–100 Hz), potentially associated with mass transport limitations or diffusion phenomena. These findings confirm the significantly lower impact of D5 on the overall electrochemical behaviour of the cell compared to sulphur-containing species.

3.4. Post-mortem characterization

A Tescan Vega 3-LaB6 Scanning Electron Microscopy (SEM) coupled with Edax Element Energy Dispersive X-ray Spectroscopy (EDX) was used for postmortem observation and analysis on the anode samples of the tested cells.

A cell tested only with Long Term Syngas (LTS) in the same conditions was used as benchmark. No microstructural modification nor detectable traces of sulphur or silicon were observed on the cells, regardless of the contaminant used (see Fig. 6). These findings suggest that the degradation observed during operation is not associated with strong chemisorption or the formation of stable reaction products on the anode. Instead, a physical adsorption mechanism (physisorption) is hypothesized, in which the contaminant species weakly interact with the anode surface. This is further supported by the cell shutdown procedure, during which a prolonged flushing with clean hydrogen reducing atmosphere (10/90 % H_2/N_2) is carried out. It is likely that this step effectively removes physisorbed species and their effects, leaving the surface chemically unaltered.

4. Conclusions

In this work, an extensive experimental investigation has been conducted to evaluate the impact of sulphur-containing compounds and a representative siloxane on solid oxide fuel cell operating with simulated bio-syngas.

Initially, SOFC samples have been tested under clean syngas conditions in a long-term polarization experiment. The results confirmed the compatibility and stability of bio-syngas as a fuel, showing only minimal voltage degradation over extended operation. Subsequently, six long-term tests have been carried out under a constant current density of 0.5 A/cm^2 by systematically introducing three different contaminants (DMS, COS, D5) to the syngas at two different concentration levels. Voltage monitoring and EIS were employed as operando diagnostic techniques to track the electrochemical response over time and identify early degradation changes. The interpretation of impedance data

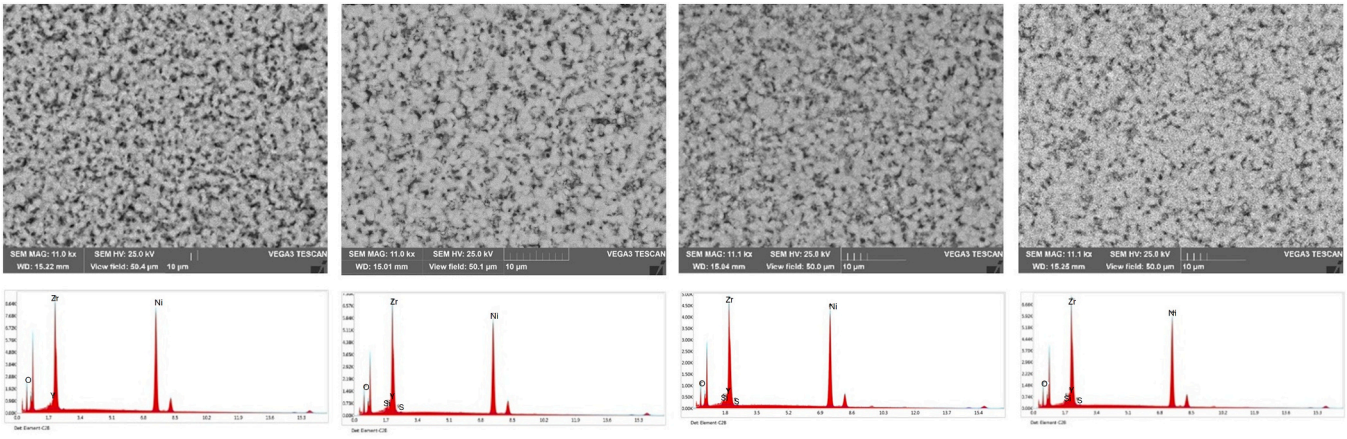

Fig. 6. Micrographs at 10 kx magnification (50 μm sample field of view) of cells tested with LTS, DMS, D5 and COS respectively and X-ray emission spectra which show no presence of the contaminants.

through equivalent circuit modelling and distribution of relaxation times provided deeper insights into the physicochemical processes driving performance loss.

The results clearly show that sulphur-containing species, even at low concentrations, induce a rapid degradation of electrochemical performance, primarily attributed to an increase in charge transfer resistance.

Although similar macroscopic behaviour is observed, it may be hypothesized that COS and DMS follow different degradation mechanisms, possibly related to their distinct molecular structures, since COS contains double bonds whereas DMS is composed only of single bonds.

In contrast, D5 appears less reactive under the same conditions. The degradation induced by D5 is more gradual and largely associated with increased mass transport limitations. This suggests progressive obstruction of the porous structure, likely due to the deposition of silica-related species, hindering gas transport to the active reaction sites.

DRT analysis proved particularly effective in isolating individual processes and identifying contaminant-specific time-dependent effects.

Post-mortem characterization using SEM and EDX analysis revealed the absence of detectable sulphur or silicon accumulation on the anode surface, suggesting the hypothesis of physisorption-dominated interactions rather than chemisorption. This finding suggests the hypothesis that inert gas purging during shutdown may assist in desorbing weakly bound species, partially restoring cell conditions.

The results show that different sulphur compounds can follow distinct reaction pathways, leading to diverse electrochemical responses. These findings may support the development of protection or regeneration strategies (e.g., desorption operations) and confirm that contaminant concentrations should remain below the levels tested, as even small amounts can affect cell performance under button-cell conditions (high flows, low fuel utilization, small area).

Further tests are planned to investigate the extent of reversibility and the potential for performance recovery following contaminant removal. In addition, future work will focus on investigating the combined effect of multiple contaminants, which is expected to provide further insight into real-world operating conditions and will be addressed in upcoming studies.

CRediT authorship contribution statement

Lucia Pera: Writing – original draft, Visualization, Methodology, Investigation, Formal analysis, Data curation, Conceptualization. **Marta Gandiglio:** Writing – review & editing, Visualization, Supervision, Methodology, Investigation, Conceptualization. **Paolo Marocco:** Writing – review & editing, Visualization, Supervision, Methodology, Investigation, Conceptualization. **Davide Pumiglia:** Writing – review & editing, Visualization, Supervision, Methodology, Investigation, Data curation, Conceptualization. **Livia Della Seta:** Writing – review & editing, Visualization, Supervision, Investigation, Data curation. **Massimo Santarelli:** Writing – review & editing, Supervision, Project administration, Funding acquisition.

Declaration of competing interest

The authors declare that they have no known competing financial interests or personal relationships that could have appeared to influence the work reported in this paper.

Acknowledgments

This research was funded by the European Union – NextGenerationEU from the Italian Ministry of Environment and Energy Security, POR H2 AdP MEES/ENEA with the involvement of the CNR and RSE, PNRR - Mission 2, Component 2, Investment 3.5 ″Ricerca e sviluppo sull'idrogeno", CUP: I83C22001170006.

Authors would like to thank Laboratorio Idrogeno e nuovi Vettori Energetici (TERIN-DEC-H2V). In particular, authors gratefully acknowledge the ENEA HotLab research group for hosting all experiments and for their experience, expertise and technical support throughout the campaign.

Appendix A. Supplementary data

Supplementary data to this article can be found online at https://doi.org/10.1016/j.jpowsour.2025.238967.

Appendix B

Table B.1
Temporal evolution of resistances for each test

	t = 0 h	t = 24 h	t = 96 h	t = 120 h
DMS = 1 ppm				
R_0 (Ω)	0.135	0.133	0.129	0.129
$R_{ct,an}$ (Ω)	0.0460	0.0544	0.0616	0.0665
$R_{ct,cat}$ (Ω)	0.0177	0.0298	0.0300	0.0158
$R_{diff,an}$ (Ω)	0.0132	0.0111	0.0165	0.0192
R_{wgs} (Ω)	0.0108	0.0188	0.0107	0.0225
DMS = 3 ppm				
R_0 (Ω)	0.0742	0.0661	0.0600	0.0622
$R_{ct,an}$ (Ω)	0.0172	0.0547	0.0561	0.0559
$R_{ct,cat}$ (Ω)	0.00413	0.00658	0.00695	0.00314
$R_{diff,an}$ (Ω)	0.00940	0.0194	0.0212	0.0243
R_{wgs} (Ω)	0.0198	0.0287	0.0248	0.0289
COS = 1 ppm				
R_0 (Ω)	0.0838	0.0847	0.0871	0.0870
$R_{ct,an}$ (Ω)	0.0535	0.0563	0.0645	0.0613
$R_{ct,cat}$ (Ω)	0.0186	0.0197	0.0317	0.0195
$R_{diff,an}$ (Ω)	0.0105	0.0160	0.0123	0.0186
R_{wgs} (Ω)	0.0352	0.0391	0.0201	0.0303

(continued on next page)

Table B.1 (*continued*)

	t = 0 h	t = 24 h	t = 96 h	t = 120 h
COS = 3 ppm				
R_0 (Ω)	0.0509	0.0514	0.0531	0.0531
$R_{ct,an}$ (Ω)	0.0567	0.0724	0.0809	0.0802
$R_{ct,cat}$ (Ω)	0.00338	0.00439	0.00668	0.00769
$R_{diff,an}$ (Ω)	0.0121	0.0156	0.00731	0.00973
R_{wgs} (Ω)	0.0291	0.0328	0.0360	0.0364
D5 = 0.7 ppm				
R_0 (Ω)	0.0535	0.0547	0.0574	0.0581
$R_{ct,an}$ (Ω)	0.0666	0.0617	0.0528	0.0565
$R_{ct,cat}$ (Ω)	0.0107	0.0233	0.0129	0.0177
$R_{diff,an}$ (Ω)	0.00442	0.00836	0.0132	0.0177
R_{wgs} (Ω)	0.0218	0.0115	0.0300	0.0119
D5 = 2 ppm				
R_0 (Ω)	0.0917	0.0925	0.0956	0.0971
$R_{ct,an}$ (Ω)	0.0465	0.0460	0.0410	0.0421
$R_{ct,cat}$ (Ω)	0.0329	0.0330	0.0300	0.0271
$R_{diff,an}$ (Ω)	0.0144	0.0154	0.0215	0.0225
R_{wgs} (Ω)	0.0202	0.0196	0.0202	0.0215

Acronyms

CEM	Controlled evaporator mixer
CNLS	Complex non linear square
COS	Carbonyl sulphide
CPE	Constant phase element
DMS	Dimethyl sulphide
DRT	Distribution relaxation times
ECM	Equivalent circuit model
EDX	Energy dispersive X-ray spectroscopy
EIS	Electrochemical impedance spectroscopy
FESEM	Field emission scanning electron microscopy
GDC	Gadolinium doped ceria
ICE	Internal combustion engine
LSC	$(La_{0.6}Sr_{0.4})CoO_{3-\delta}$
LTS	Long Term Syngas
MFC	Mass flow controller
OCV	Open Circuit Voltage
SEM	Scanning electron microscopy
SOFC	Solid oxide fuel cell
TPB	Triple phase boundary
WGS	Water gas shift
YSZ	Yttria stabilized zirconia

Data availability

Data will be made available on request.

References

[1] M. Gandiglio, P. Marocco, A. Nieminen, M. Santarelli, J. Kiviaho, Energy and environmental performance from field operation of commercial-scale SOFC systems, Int. J. Hydrogen Energy 85 (2024) 997–1009, https://doi.org/10.1016/j.ijhydene.2024.08.332.

[2] A.B. Stambouli, E. Traversa, A. Stambouli, Solid oxide fuel cells (SOFCs): a review of an environmentally clean and efficient source of energy. www.elsevier.com/locate/rser, 2002.

[3] A. Lanzini, H. Madi, V. Chiodo, D. Papurello, S. Maisano, M. Santarelli, J. Van herle, Dealing with fuel contaminants in biogas-fed solid oxide fuel cell (SOFC) and molten carbonate fuel cell (MCFC) plants: degradation of catalytic and electro-catalytic active surfaces and related gas purification methods, Prog. Energy Combust. Sci. 61 (2017) 150–188, https://doi.org/10.1016/j.pecs.2017.04.002.

[4] L. Pera, M. Gandiglio, P. Marocco, D. Pumiglia, M. Santarelli, Trace contaminants in biogas: biomass sources, variability and implications for technology applications, J. Environ. Chem. Eng. 12 (2024), https://doi.org/10.1016/j.jece.2024.114478.

[5] D.D. Papadias, S. Ahmed, R. Kumar, Fuel quality issues with biogas energy - an economic analysis for a stationary fuel cell system, Energy 44 (2012) 257–277, https://doi.org/10.1016/j.energy.2012.06.031.

[6] G. Pongratz, V. Subotić, H. Schroettner, C. Hochenauer, M. Skrzypkiewicz, J. Kupecki, A. Anca-Couce, R. Scharler, Analysis of H2S-related short-term degradation and regeneration of anode- and electrolyte supported solid oxide fuel cells fueled with biomass steam gasifier product gas, Energy 218 (2021), https://doi.org/10.1016/j.energy.2020.119556.

[7] D. Papurello, A. Lanzini, SOFC single cells fed by biogas: experimental tests with trace contaminants, Waste Manag. 72 (2018) 306–312, https://doi.org/10.1016/j.wasman.2017.11.030.

[8] K. Sasaki, K. Susuki, A. Iyoshi, M. Uchimura, N. Imamura, H. Kusaba, Y. Teraoka, H. Fuchino, K. Tsujimoto, Y. Uchida, N. Jingo, H[sub 2]S poisoning of solid oxide fuel cells, J. Electrochem. Soc. 153 (2006) A2023, https://doi.org/10.1149/1.2336075.

[9] P. Boldrin, E. Ruiz-Trejo, J. Mermelstein, J.M. Bermúdez Menéndez, T. Ramírez Reina, N.P. Brandon, Strategies for carbon and sulfur tolerant solid oxide fuel cell materials, incorporating lessons from heterogeneous catalysis, Chem. Rev. 116 (2016) 13633–13684, https://doi.org/10.1021/acs.chemrev.6b00284.

[10] T. Aworinde, W. Yang, L. Mathur, V. Ashokan, S. Sengodan, A review of electrode poisoning in fuel cells: strategies for mitigation and performance enhancement, J. Power Sources 655 (2025), https://doi.org/10.1016/j.jpowsour.2025.237901.

[11] A. Hagen, J.F.B. Rasmussen, K. Thydén, Durability of solid oxide fuel cells using sulfur containing fuels, J. Power Sources (2011) 7271–7276, https://doi.org/10.1016/j.jpowsour.2011.02.053.

[12] A. Hauch, A. Hagen, J. Hjelm, T. Ramos, Sulfur poisoning of SOFC anodes: effect of overpotential on long-term degradation, J. Electrochem. Soc. 161 (2014) F734–F743, https://doi.org/10.1149/2.080406jes.

[13] R.J. Spiegel, J.L. Preston, Test results for fuel cell operation on anaerobic digester gas. www.elsevier.comrlocaterjpowsour, 2000.

[14] H. Yu, C. Frantz, L. Savioz, P. Aubin, D. Fronterotta, C. Geipel, H. Moussaoui, G. Jeanmonod, L. Wang, J. Van herle, Poisoning and recovery behavior of Ni-GDC based electrolyte-supported solid oxide fuel cell exposed to common sulfur

compounds under processed biogas environment, J. Power Sources 642 (2025), https://doi.org/10.1016/j.jpowsour.2025.236901.
[15] H. Madi, A. Lanzini, S. Diethelm, D. Papurello, J. Van Herle, M. Lualdi, J. Gutzon Larsen, M. Santarelli, Solid oxide fuel cell anode degradation by the effect of siloxanes, J. Power Sources 279 (2015) 460–471, https://doi.org/10.1016/j.jpowsour.2015.01.053.
[16] H. Madi, S. Diethelm, S. Poitel, C. Ludwig, J. Van herle, Damage of siloxanes on Ni-YSZ anode supported SOFC operated on hydrogen and bio-syngas, in: Fuel Cells, John Wiley and Sons Ltd, 2015, pp. 718–727, https://doi.org/10.1002/fuce.201400185.
[17] K. Sasaki, K. Haga, T. Yoshizumi, D. Minematsu, E. Yuki, R. Liu, C. Uryu, T. Oshima, T. Ogura, Y. Shiratori, K. Ito, M. Koyama, K. Yokomoto, Chemical durability of solid oxide fuel cells: influence of impurities on long-term performance, J. Power Sources 196 (2011) 9130–9140, https://doi.org/10.1016/j.jpowsour.2010.09.122.
[18] A. Weber, S. Dierickx, A. Kromp, E. Ivers-Tiffée, Sulfur poisoning of anode-supported SOFCs under reformate operation, Fuel Cells 13 (2013) 487–493, https://doi.org/10.1002/fuce.201200180.
[19] A. Hagen, Sulfur poisoning of the water gas shift reaction on anode supported solid oxide fuel cells, J. Electrochem. Soc. 160 (2013) F111–F118, https://doi.org/10.1149/2.060302jes.
[20] J.H. Kim, M. Liu, Y. Chen, R. Murphy, Y.M. Choi, Y. Liu, M. Liu, Understanding the impact of sulfur poisoning on the methane-reforming activity of a solid oxide fuel cell anode, ACS Catal. 11 (2021) 13556–13566, https://doi.org/10.1021/acscatal.1c02470.
[21] Waste2Watts Project, Unlocking Unused bio-WASTE Resources with Low Cost Cleaning and Thermal Integration with Solid Oxide Fuel Cells, 2020.
[22] A. Kromp, A. Leonide, A. Weber, E. Ivers-Tiffée, Electrochemical analysis of reformate-fuelled anode supported SOFC, J. Electrochem. Soc. 158 (2011) B980, https://doi.org/10.1149/1.3597177.
[23] J. Ma, Y. Jiang, P.A. Connor, S.R. Gamble, M. Cassidy, C. Jiang, J.T.S. Irvine, Detailed study of sulfur poisoning and recovery of Ni-YSZ-Based anodes operating up to 1.8 W cm-2in a biogas fuel, Int. J. Energy Res. 2023 (2023), https://doi.org/10.1155/2023/2339117.
[24] C. Boigues Muñoz, D. Pumiglia, S.J. McPhail, D. Montinaro, G. Comodi, G. Santori, M. Carlini, F. Polonara, More accurate macro-models of solid oxide fuel cells through electrochemical and microstructural parameter estimation - part I: experimentation, J. Power Sources 294 (2015) 658–668, https://doi.org/10.1016/j.jpowsour.2015.06.118.
[25] C. Boigues-Muñoz, Computational Simulation of Solid Oxide Fuel Cells – Integrating Numerical and Experimental Approaches, 2015. https://iris.univpm.it/handle/11566/242989.
[26] A. Leonide, V. Sonn, A. Weber, E. Ivers-Tiffée, Evaluation and modeling of the cell resistance in anode-supported solid oxide fuel cells, J. Electrochem. Soc. 155 (2008) B36, https://doi.org/10.1149/1.2801372.
[27] A. Kromp, Model-Based Interpretation of the Performance and Degradation of Reformate Fueled Solid Oxide Fuel Cells, 2013. https://publikationen.bibliothek.kit.edu/1000034160.
[28] A. Leonide, SOFC Modelling and Parameter Identification by Means of Impedance Spectroscopy, 2010. https://publikationen.bibliothek.kit.edu/1000019173.
[29] D. Pumiglia, Intermediate Temperature Solid Oxide Fuel Cells Fed with Syngas: an Evaluation of Electrochemical Phenomena, 2017.
[30] Scribner, ZView software for windows, (n.d.). https://www.scribner.com/software/68-general-electrochemistr376-zview-for-windows/(accessed August 28, 2025).
[31] X. Wu, Y. Tian, X. Zhou, X. Kong, J. Zhang, W. Zuo, D. Wang, X. Ye, Performance and long-term stability of nickel/yttria-stabilized zirconia anode-supported solid oxide fuel cell in simulated biosyngas, Energy 114 (2016) 1–9, https://doi.org/10.1016/j.energy.2016.07.160.
[32] C. Comminges, Q.X. Fu, M. Zahid, N.Y. Steiner, O. Bucheli, Monitoring the degradation of a solid oxide fuel cell stack during 10,000 h via electrochemical impedance spectroscopy, Electrochim. Acta 59 (2012) 367–375, https://doi.org/10.1016/j.electacta.2011.10.080.
[33] R. Suwanwarangkul, E. Croiset, E. Entchev, S. Charojrochkul, M.D. Pritzker, M. W. Fowler, P.L. Douglas, S. Chewathanakup, H. Mahaudom, Experimental and modeling study of solid oxide fuel cell operating with syngas fuel, J. Power Sources 161 (2006) 308–322, https://doi.org/10.1016/j.jpowsour.2006.03.080.
[34] V. Subotić, A. Baldinelli, L. Barelli, R. Scharler, G. Pongratz, C. Hochenauer, A. Anca-Couce, Applicability of the SOFC technology for coupling with biomass-gasifier systems: Short- and long-term experimental study on SOFC performance and degradation behaviour, Appl. Energy 256 (2019), https://doi.org/10.1016/j.apenergy.2019.113904.
[35] S. Zhao, H. Yi, X. Tang, S. Jiang, F. Gao, B. Zhang, Y. Zuo, Z. Wang, The hydrolysis of carbonyl sulfide at low temperature: a review, Sci. World J. 2013 (2013), https://doi.org/10.1155/2013/739501.
[36] S. Renda, E. Palo, M. Colozzi, V. Palma, Carbonyl sulfide removal from refinery tail-gas streams: experimental and kinetic study of the hydrolysis reaction, Sep. Purif. Technol. 324 (2023), https://doi.org/10.1016/j.seppur.2023.124417.
[37] K. Yang, J. Chen, J. Mi, R. Yin, J. Yuan, J. Shi, G. Wang, J. Li, More than just a reactant: H2O promotes carbonyl sulfide hydrolysis activity over Ni-MgAl-LDO by inhibiting H2S poisoning, Fuel 333 (2023), https://doi.org/10.1016/j.fuel.2022.126503.
[38] J. Tian, R.J. Milcarek, Siloxane deposition on the Ni-YSZ solid oxide fuel cell anode exposed to bio-syngas, J. Electrochem. Soc. 168 (2021) 044503, https://doi.org/10.1149/1945-7111/abf21a.
[39] J. Tian, R.J. Milcarek, Investigating the degradation mechanism of the solid oxide fuel cell nickel-yttria stabilized zirconia anode under siloxane contamination, J. Power Sources 480 (2020), https://doi.org/10.1016/j.jpowsour.2020.229122.
[40] K. Haga, S. Adachi, Y. Shiratori, K. Itoh, K. Sasaki, Poisoning of SOFC anodes by various fuel impurities, Solid State Ionics 179 (2008) 1427–1431, https://doi.org/10.1016/j.ssi.2008.02.062.
[41] P. Caliandro, Identification of Solid Oxide Cell Elementary Processes by Electrochemical Impedance Spectroscopy, 2018.